International Journal of Latest Engineering Research and Applications (IJLERA) ISSN: 2455-7137

Volume – 04, Issue – 04, April 2019, PP – 34-45

Image based fractal characterization and modeling of multiphase flow in sandstone formation

[1]Usman, A.H., [2]Zhou, Y.

[1]*Department of Chemical Engineering, Ahmadu Bello University, Nigeria*
[2]*Department of Petroleum Engineering, University of Aberdeen, United Kingdom*

Abstract: Fractal-based approach has been reported to be very promising in the study of fluid transport in porous media. It has been discovered that, by treating the pores in sandstone formation as a set of fractals, a significant information regarding the mechanisms of multiphase flow in porous media can be unveiled. Consequently, a great attention has recently been focused on the use of fractal theory to develop analytical models for flow parameters in porous media. Hence, in this work, a similar concept of fractal theory was employed to characterize the pore spaces in a 2-dimensional image of Bentheimersandstone. Based on the analysis, the apertures were found to be fractals in nature with pore area and tortuosity fractal dimensions of 1.58 and 1.14 respectively. Also, fractal-based analytical functions have been derived for capillary pressure and relative permeability. The formulated flow functions have shown that the capillary pressure and permeability in a given fractal porous media depend not only on saturation, but also on several other parameters such as wettability, minimum and maximum pore size as well as fractal dimensions. Moreover, a permeability model that incorporates film/layer thickness has been proposed and validated using existing experimental data of the Bentheimer sandstone and theresults were found to be consistent with both experimental and numerical figures especially for the nonwetting phase.

Keywords: Capillary pressure, fractal, multiphase flow, porous media, relative permeability.

1. Introduction

It is undoubtedly agreed that the idea of fractal geometry which was introduced and pioneered by Mandelbrot in the early 80s plays an unprecedented role in the study of porous media [1]. The word fractal simply means a repeating geometrical pattern that is often being exhibited by some natural and synthetic objects. The application of this concept of fractal theory in modeling transport properties in porous media has been a great breakthrough of the last few decades. This follows some experimental findings on certain samples of sandstones (porous media). The samples were examined through the use of scanning electron microscopy (SEM) and their apertures were found to be fractals in nature spanning over 3 to 4 orders of magnitude from 1nm to 100μm [2-7]. Since then, several researchers have been using this concept in order to understand the nature of multiphase flow characteristics in fractal porous media[1]. And a significant number of fractal-based relative permeability and capillary pressure models have been proposed and the models revealed that the transport properties of a porous media are functions of several microscopic parameters such as pore size, pore area, and tortuosity fractal dimensions [5]. Also, despite the several assumptions and simplifications, the derived analytical functions were found to bepromising and less time-demanding when solving them computationally.

Similarly, a lot of empirical correlations have also been formulated to study the flow in porous media, but many of them could not account for the complexity of the micro structural arrangements in the formation. Empirical models such as the popular Brooks-Corey's which are hitherto used for quantification of relative permeability have been proved to be applicable only, to homogeneous and consolidated sandstones [8]. Also, an overwhelming majority of the experimental and numerical results are often presented with empirical correlations that contain some constants whose physical meanings cannot be explained. Consequently, some researchers have attempted to develop generalized analytical models with better physical definitions that will help address the problem of multiphase flows in porous media. One of such vital studies that demonstrated the applicability of fractal theory in the formulation of analytical flow functions was carried out by Yu and Liu [9]. They derived permeability and relative permeability expressions for single and multiphase flow systems. Based on their models, they concluded that multiphase flow functions depend not only on saturation of a flowing phase but also on tortuosity and pore fractal dimensions of a porous media. However, their models only consider the effects of fractal dimensions and porosity but neglected other important factors such as wettability and capillary pressure [4].

Also, by treating porous media as consisting of tortuous capillaries, Tan et al. [4] derived a fractal-based analytical model for relative permeability during transient flow process, and they discovered that the

model was in accord with experimentally reported findings. Moreover, Tan et al. [10] formulated another permeability model that shows how microstructural parameters in bi-fractal porous media influences the mechanisms of fluid flow. They contend that, unlike other empirical models that are often characterized by some trivial constants, their relative permeability model consists only of physically meaningful parameters. However, despite agreeing with existing results, the model did not consider the impact of other influencing properties such as wettability and capillary pressure. Additionally, although the formulated function proved to be valid during a transient period, studies have revealed that a porous media especially petroleum reservoirs spend a very little time in the transient situation. Therefore, it may not necessarily be applicable to other non-time dependent conditions.

Furthermore, quite a number of published works have only been able to validate their formulated models based on the assumption of uniform wetting in the porous media which rarely exist in nature. Hence, to better characterize and understand the mechanisms of multiphase flow in porous materials, there is a need for more research to be done. It is also pertinent to consider real data extracted directly from actual porous media image than to assume a hypothetical value as it may not necessarily depict the desired trend expected from a real rock. And a suggested approach from several pieces of research for predicting closed to reality behavior in a given porous media is to study its structure as a set of fractals [7]. Therefore, this work adopted a similar concept of fractal theory on a 2-dimensional image of Bentheimersandstone in order to extract micro structural data and formulate better expressions for multiphase flow parameters in sandstones. The developed fractal-based relations were further modified to incorporate the effect of film thickness which affects the flow of fluid through the apertures of a porous media.

In essence, it is worthy to note that the underlying idea behind the use of fractal theory to study flow through porous media stemmed from the work of Yu and Cheng [11]. They proposed the fractal scaling law to describe the distribution of pores in porous media as given by equations 1 and 2:

$$(L \geq N) = \left(\frac{\lambda_{max}}{\lambda}\right)^{D_f} \quad (1)$$

where N is the cumulative number of the capillaries, λ is the size of the pore (pore diameter), and D_f is the fractal dimension. They also found that in porous media, the pore openings are not straight but tortuous and came up with another fractal scaling law for capillary length as a function of tortuosity as given by (2):

$$L_T(\lambda) = \lambda^{1-D_T} L_s^{D_T} \quad (2)$$

where D_T is the tortuosity dimension, L_T and Ls are tortuous and straight length of the capillaries respectively. (2) clearly shows that the two lengths can only be equal if the tortuosity dimension is unity [11].The aforementioned equations have been the lifeline in the application of the concept of fractal geometry in developing extended equations for multiphase flow in porous media.

2. Processing of the 2D SEM image

Since numerous studies have shown that most porous materials can be treated as fractals and that fractal scaling law can be used to represent such exactly or statistically self-similar objects [3,7], it is pertinent to adopt amethodology that will accurately help determine the fractal characterization parameters. Hence, a theoretically reported method that can reliably be used to first process SEM image prior to pore data retrieval involves the use of image processing software called *Image J.* The procedure is briefly depicted in fig.1a and the processed image is shown in fig.1b.

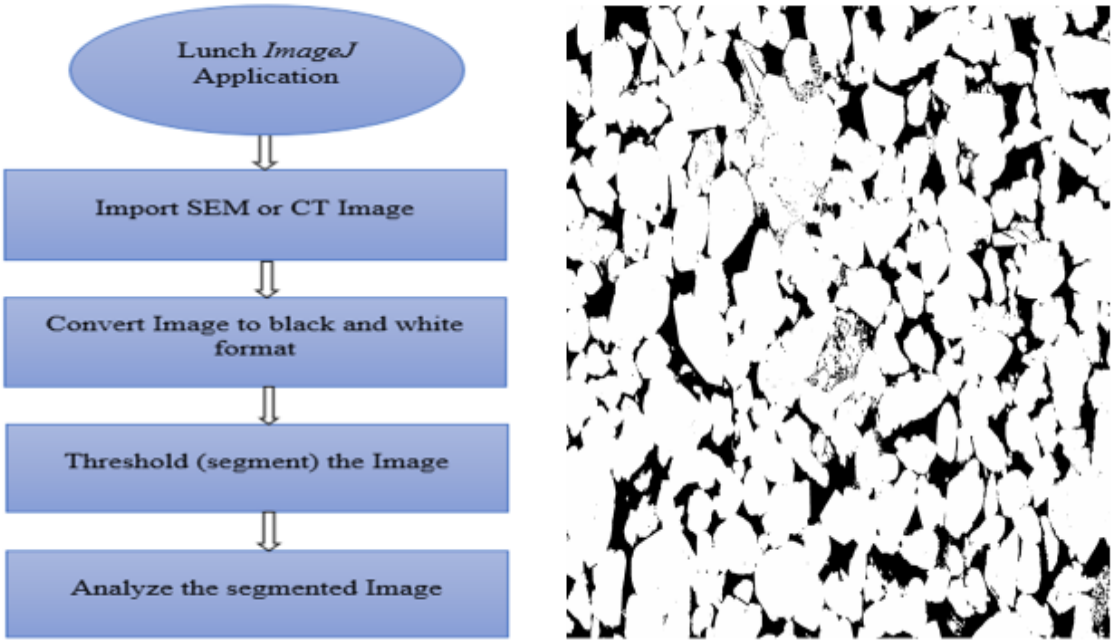

Figure 1: (a) Image processing procedure. (b) Processed 2D SEM image of Bentheimer sandstone

3. Extraction of pore data using box counting technique in MATLAB

Box-counting is a MATLAB based method that is widely utilized by many researchers for the evaluation of fractal dimensions. Yu and Cheng [11] in their work to formulate a fractal model for computation of permeability of a bi-dispersed porous media, applied this method to compute both pore area and tortuosity fractal dimensions. Also, Chen and Yao [12] employed the box-counting method for the quantification of fractal dimension in their attempt to derive and validate an improved permeability model for a low permeable media. Similarly, Liu et al. [13] used this algorithm to determine the fractal dimension of fractures in rock masses and found that the result agreed well with existing theoretical values. Therefore, after establishing the efficacy and reliability of this method from various published literature, this work adopted a similar approach in the computation of the fractal dimensions from 2D image of the Bentheimer sandstone sample.

The method is applied to the processed image using a MATLAB code that accomplishes the process within a very short time frame and returns the output based on user specified feedback. The process involves rearrangement and linearization of the fractal scaling law given in (1) as given below by (3):

$$\ln(N) = D_f \ln\left(\frac{1}{\gamma}\right) + \mathrm{b} \qquad (3)$$

where N denotes the number of boxes counted, D_f is the fractal dimension, γ (same as λ) is box size, and b is a constant representing the intercept on vertical axis. The algorithm refers to the pores as pixels and determines the number of boxes that can be used to cover such pixels. The output is returned as a linear log-log plot of number of boxes versus size with the slope (D_f) delineating fractal characteristic of the image as in fig.2. The tortuosity fractal dimension (D_T) was similarly obtained from the box-counting method.

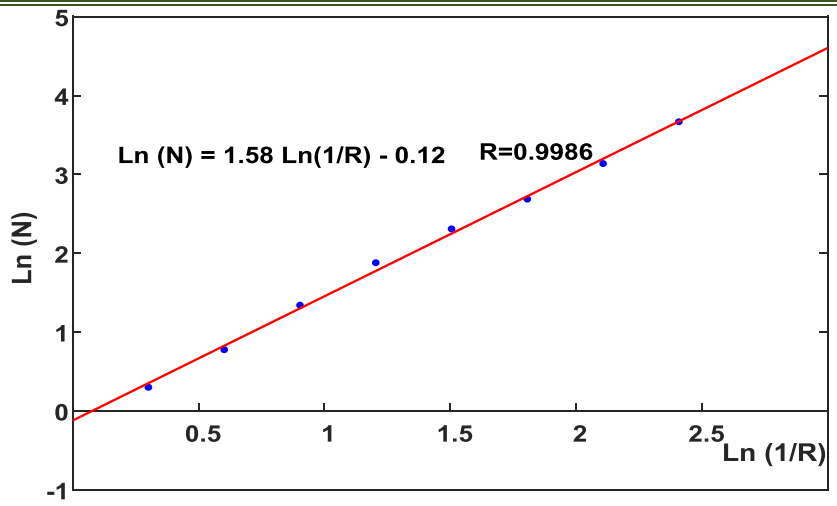

Figure 2: Graphical demonstration of fractal scaling law using box counting algorithm

4. Formulation of analytical models for flow through fractal porous media

Generally, the formulation of fractal-based flow equations for fluid flow in porous media involve the use of fractal theory and the prominent Hagen-Poiseuille (H-P) equation [9,11,14]. However, in this work a modified form of H-P equation, Henry Darcy's law, and fractal scaling law were combined to model multiphase flow in sandstone (porous medium).

The fractal scaling law which gives a relationship between cumulative number of pores in fractal porous media and their size as proposed by Yu and Cheng [11] is given by (1). From that equation, the total number of pore spaces or alternatively referred to as pore population can be obtained when λ is minimum and the function can be expressed as:

$$N_t(L \geq \lambda) = (\frac{\lambda_{max}}{\lambda_{min}})^{D_f} \quad (4)$$

Differentiating equation 1 between λ and λ + dλ, we obtained [9]:

$$-dN = \lambda_{max}^{D_f} \lambda^{-1-D_f} D_f d\lambda. \quad (5)$$

The negative sign in front of dN shows that the population of the pores reduces as theirsize increase [9] and this is concomitant with a generally accepted physical situation. To get the probability density function, we can divide equation 5 by 4 to get;

$$-\frac{dN}{N_t} = D_f \lambda_{min}^{D_f} \lambda^{-(1+D_f)} d\lambda \quad (6)$$

And,

$$f(\lambda) = D_f \lambda_{min}^{D_f} \lambda^{-(1+D_f)} \quad (7)$$

The probability function is shown in equation (8) as given by [11]:

$$\int_{-\infty}^{\infty} f(\lambda) \mathrm{d}\lambda = 1 \quad (8)$$

Therefore, plugging (7) into (8) with lower and upper limits of integration corresponding to λ_{min} and λ_{max}, the integral was evaluated to obtain

$$-\int_{\lambda_{min}}^{\lambda_{max}} D_f \lambda_{min}^{D_f} \lambda^{-(1+D_f)} \mathrm{d}\lambda = 1 - (\frac{\lambda_{min}}{\lambda_{max}})^{D_f} \quad (9)$$

However, it could be seen from equation (9) that the probability theory function of (8) can only be applicable if the second term on the right-hand part of (9) is zero. Fortunately, several studies have shown that in a fractal porous media $\frac{\boldsymbol{\lambda_{min}}}{\boldsymbol{\lambda_{max}}}$ is usually less than 10^{-2} [3,5,11,12]. Also, if the minimum pore dimension tends towards the maximum size, equation 9 will be equal to zero and the porous media cannot be regarded as being fractal as it has failed to satisfy the requisite criteria. Hence, for a porous media to be regarded and treated as fractal it must satisfy equation 10 as given by [11]:

$$(\frac{\lambda_{min}}{\lambda_{max}})^{D_f} \approx 0 \quad (10)$$

And based on the analysis of the pore size distribution of Bentheimer sandstone used in this work, it was found to be fractal and satisfied the aforementioned criteria. As a result, the concept of fractal theory was employed to model multiphase flow in this porous media as presented in the following sub-sections.

4.1 Formulation of relative permeability model

The capillary openings in real porous media are not usually straight as is assumed in most studies. The assumption is usually made for the sake of simplicity. Therefore, in this work, tortuosity was considered in order to derive a complete representative model which can at any time be reduced to the conventional straight tube model as that will only be a matter of assuming D_T to be unity.

The flow through each path can be represented by popular Hagen-Poiseuille (H-P) equation as expressed in [15]:

$$q = G\frac{\pi\lambda^4}{128\mu}\frac{\Delta P}{L_T(\lambda)} \tag{11}$$

where q represents flow rate, G is a geometrical factor and is 1 for circular capillaries [15], ΔP is a total pressure drop, L_t denotes length of capillaries, and μ is viscosity of the fluid. The total pressure drop comprises of the capillary pressure between the phases and overall pressure difference across a given capillary tube [6]. The capillary pressure as a function of pore size and porosity in a porous material is given in equation 3.12 [16,17] as:

$$P_c = \frac{4\sigma cos\theta}{\lambda}\frac{1-\emptyset}{\emptyset} \tag{12}$$

By substituting all the foregoing conditions into (11), the flow through a single capillary is obtained as follows:

$$q(\lambda) = \frac{\pi}{128\mu L_s^{D_T}}[\Delta P\lambda^{3+D_T} + (4\sigma cos\theta\frac{1-\emptyset}{\emptyset})\lambda^{2+D_T}] \tag{13}$$

The total flow rate over an entire section of a given porous media cell can be obtained by summing up the individual flow contributed by each capillary tube from smallest to the largest. Thus:

$$Q = -\int_{\lambda_{min}}^{\lambda_{max}} q(\lambda)\mathrm{dN}(\lambda) \tag{14}$$

where Q denotes the total flowrate. By plugging (5) and (13) into (14), integrating and simplifying, the total flow becomes

$$Q = \frac{\pi D_f}{128\mu L_s^{D_T}}\left[\frac{\Delta P\lambda_{max}^{3+D_T}}{3+D_T-D_f}\left(1-\left(\frac{\lambda_{min}}{\lambda_{max}}\right)^{3+D_T-D_f}\right) + \frac{4\sigma cos\theta\,(\frac{1-\emptyset}{\emptyset})}{(2+D_T-D_f)}\lambda_{max}^{2+D_T}\left(1-(\frac{\lambda_{min}}{\lambda_{max}})^{2+D_T-D_f}\right)\right]. \tag{15}$$

However, since both D_f and D_T lies between 1 and 2 and the ratio $\lambda_{min}/\lambda_{max}$ <10^{-2}, and also $(\frac{\lambda_{min}}{\lambda_{max}})^{D_f} \approx 0$) for a fractal porous media [11], then (15) can further be simplified to:

$$Q = \frac{\pi D_f}{128\mu L_s^{D_T}}\left[\frac{\Delta P\lambda_{max}^{3+D_T}}{3+D_T-D_f} + \frac{4\sigma cos\theta\,(\frac{1-\emptyset}{\emptyset})}{(2+D_T-D_f)}\lambda_{max}^{2+D_T}\left(1-(\frac{\lambda_{min}}{\lambda_{max}})^{2+D_T-D_f}\right)\right] \tag{16}$$

Similarly, the total flow rate through a given unit cell in a porous media can be determine using a simplified form of Darcy's law. Hence, combining that (16) with Darcy's law, the permeability K of porous media can be expressed as:

$$K = \frac{\pi D_f L_S^{1-D_T}}{128A}\left[\frac{\lambda_{max}^{3+D_T}}{3+D_T-D_f} + \frac{4\sigma cos\theta\,(\frac{1-\emptyset}{\emptyset})}{(2+D_T-D_f)\Delta P}\lambda_{max}^{2+D_T}\left(1-(\frac{\lambda_{min}}{\lambda_{max}})^{2+D_T-D_f}\right)\right] \tag{17}$$

It is however relevant to mention that the foregoing derivation of the porous media conductance was based on several assumptions. Also, the pore area A_p available for flow in a fractal porous media with circular capillary openings can be obtained as follows [10,12]:

$$A_p = \int_{\lambda_{min}}^{\lambda_{max}}\frac{\pi}{4}\lambda^2(-\mathrm{dN}) \tag{18}$$

And the total area A of a unit cell under consideration can be determined using:

$$A = \frac{A_p}{\emptyset} = \frac{\int_{\lambda_{min}}^{\lambda_{max}}\frac{\pi}{4}\lambda^2(-\mathrm{dN})}{\emptyset} = \frac{\pi D_f\lambda_{max}^2}{4(2-D_f)\emptyset}\left(1-(\frac{\lambda_{min}}{\lambda_{max}})^{2-D_f}\right) \tag{19}$$

However, $(\frac{\lambda_{min}}{\lambda_{max}})^{2-D_f}$ represents porosity $\emptyset$ in a porous media [3]. As a result, (19) becomes:

$$A = \frac{\pi D_f\lambda_{max}^2}{4(2-D_f)}\left(\frac{1-\emptyset}{\emptyset}\right) \tag{20}$$

By substituting (20) into (17), the permeability is expressed as follows:

$$K = \frac{4(2-D_f)\emptyset L_S^{1-D_T}\lambda_{max}^{D_T}}{128(1-\emptyset)}\left[\frac{\lambda_{max}}{3+D_T-D_f} + \frac{4\sigma cos\theta\,(\frac{1-\emptyset}{\emptyset})}{(2+D_T-D_f)\Delta P}\left(1-(\frac{\lambda_{min}}{\lambda_{max}})^{2+D_T-D_f}\right)\right] \tag{21}$$

(21) is used for computation of permeability in fractal porous media. And it is obvious that the permeability in a fractal porous media is a function of microstructural properties.

However, to determine the permeability of a given phase in a porous media (21) can be modified using the following relationships [14]:

$$\emptyset_{\boldsymbol{w}} = \boldsymbol{S_w}\emptyset \qquad (22a)$$

$$\boldsymbol{\lambda_{min,w}} = \boldsymbol{\lambda_{min}}\boldsymbol{S_w}^{\frac{1}{2}} \qquad (22b)$$

$$\boldsymbol{\lambda_{max,w}} = \boldsymbol{\lambda_{max}}\boldsymbol{S_w}^{\frac{1}{2}} \qquad (22c)$$

$$\boldsymbol{D_{f,W}} = \boldsymbol{2} - \frac{\boldsymbol{ln\emptyset S_w}}{\boldsymbol{ln\left(\frac{\lambda_{min,w}}{\lambda_{max,w}}\right)}} \qquad (22d)$$

where S and subscript w mean saturation and wetting phase respectively. Therefore, by plugging the foregoing relations into (21), the phase permeability can be obtained as:

$$K_W = \frac{4(2-D_{f,w})\emptyset L_S^{1-D_T}\lambda_{max}^{D_T}}{128(1-S_w\emptyset)}\left[\frac{\lambda_{max}\sqrt{S_w}}{3+D_T-D_{f,w}} + \frac{4\sigma cos\theta\,(\frac{1-S_w\emptyset}{S_w\emptyset})}{(2+D_T-D_{f,w})\Delta P}\left(1-(\frac{\lambda_{min}}{\lambda_{max}})^{2+D_T-D_{f,w}}\right)\right]S_w^{\frac{(D_T+2)}{2}} \qquad (23)$$

Similarly, the permeability of the non wetting medium (nw) can be presented as:

$$K_{nw} = \frac{4(2-D_{f,nw})\emptyset L_S^{1-D_T}\lambda_{max}^{D_T}}{128(1-S_{nw}\emptyset)}\left[\frac{\lambda_{max}\sqrt{S_{nw}}}{3+D_T-D_{f,nw}} + \frac{4\sigma cos\theta\,(\frac{1-S_{nw}\emptyset}{S_{nw}\emptyset})}{(2+D_T-D_{f,nw})\Delta P}\left(1-(\frac{\lambda_{min}}{\lambda_{max}})^{2+D_T-D_{f,nw}}\right)\right](S_{nw})^{\frac{(D_T+2)}{2}} \qquad (24)$$

Therefore, based on the Darcy's law for multiphase flow, the relative permeability (K_r) model for each phase can be derived as follows [18]:

$$K_{rw} = \frac{K_w}{K}, \quad K_{r,nw} = \frac{K_{nw}}{K} \qquad (25)$$

Hence, by using (17), (23), and (24) into (25), the relative permeability for each phase can be expressed as follows:

$$K_{rw} = \frac{\frac{2-D_{f,w}}{1-S_w\emptyset}\left[\frac{\lambda_{max}\sqrt{S_w}}{3+D_T-D_{f,w}} + \frac{4\sigma cos\theta\,(\frac{1-S_w\emptyset}{S_w\emptyset})}{(2+D_T-D_{f,w})\Delta P}\left(1-(\frac{\lambda_{min}}{\lambda_{max}})^{2+D_T-D_{f,w}}\right)\right]S_w^{\frac{(D_T+2)}{2}}}{\frac{(2-D_f)}{(1-\emptyset)}\left[\frac{\lambda_{max}}{3+D_T-D_f} + \frac{4\sigma cos\theta\,(\frac{1-\emptyset}{\emptyset})}{(2+D_T-D_f)\Delta P}\left(1-(\frac{\lambda_{min}}{\lambda_{max}})^{2+D_T-D_f}\right)\right]} \qquad (26)$$

$$K_{r,nw} = \frac{\frac{(2-D_{f,nw})}{(1-S_{nw}\emptyset)}\left[\frac{\lambda_{max}\sqrt{S_{nw}}}{3+D_T-D_{f,nw}} + \frac{4\sigma cos\theta\,(\frac{1-S_{nw}\emptyset}{S_{nw}\emptyset})}{(2+D_T-D_{f,nw})\Delta P}\left(1-(\frac{\lambda_{min}}{\lambda_{max}})^{2+D_T-D_{f,nw}}\right)\right](S_{nw})^{\frac{(D_T+2)}{2}}}{\frac{(2-D_f)}{(1-\emptyset)}\left[\frac{\lambda_{max}}{3+D_T-D_f} + \frac{4\sigma cos\theta\,(\frac{1-\emptyset}{\emptyset})}{(2+D_T-D_f)\Delta P}\left(1-(\frac{\lambda_{min}}{\lambda_{max}})^{2+D_T-D_f}\right)\right]} \qquad (27)$$

(26) and (27) revealed that relative permeability depends not only on saturation but also on microstructure properties. And the interesting aspect of these multiphase functions is that they are free of empirical constants and all the parameters have their physical meaning.

4.2 Capillary pressure model

Capillary pressure is a very critical parameter in modeling flow of fluid in porous media. To model this important flow parameter, the following relation is used [17,19]:

$$P_{C,avg} = \int_{\lambda_{min}}^{\lambda_{max}} P_C f(\lambda)\mathrm{d}\lambda \qquad (28)$$

where $P_{C,avg}$ represents the capillary pressure average over the entire capillaries. By utilizing (7) and (12) into (28) and integrating the function over the set limits, the average P_C, is obtained as:

$$P_{C,avg} = \int_{\lambda_{min}}^{\lambda_{max}} \frac{4\sigma cos\theta}{\lambda}\frac{1-\emptyset}{\emptyset}D_f\lambda_{min}^{D_f}\lambda^{-(1+D_f)}\,d\lambda = \frac{4\sigma cos\theta}{\lambda_{min}}\frac{1-\emptyset}{\emptyset}\frac{D_f}{D_f+1} \qquad (29)$$

And by using the definitions presented in (22a-c) and simplifying, the average P_C for a wetting phase is presented as:

$$P_{C,w} = \frac{4\sigma cos\theta}{\lambda_{min}}\frac{1-S_w\emptyset}{\emptyset}\left[\frac{2ln\left(\frac{\lambda_{min}}{\lambda_{max}}\right)-\ln(S_w\emptyset)}{3ln\left(\frac{\lambda_{min}}{\lambda_{max}}\right)-\ln(S_w\emptyset)}\right]S_w^{-\frac{3}{2}} \qquad (30a)$$

Similarly, with respect to nonwetting (nw) medium, the average P_C is given as:

$$P_{C,nw} = \frac{4\sigma cos\theta}{\lambda_{min}}\frac{1-S_{nw}\emptyset}{\emptyset}\left[\frac{2ln\left(\frac{\lambda_{min}}{\lambda_{max}}\right)-\ln(S_{nw}\emptyset)}{3ln\left(\frac{\lambda_{min}}{\lambda_{max}}\right)-\ln(S_{nw}\emptyset)}\right]S_{nw}^{-\frac{3}{2}} \qquad (30b)$$

(30a) and (30b) clearly indicate that capillary pressure is a function of not just saturation but also the micro structural parameters of the porous media.

4.3 Modified permeability model incorporating film thickness

The phase permeability model derived earlier is extended here to account for the effect of layer or film thickness that can be formed during multiphase flow in porous media. This extension is made in analogy to what normally happens during flow in nanotubes. In simple terms, film thickness refers to the layer formed by

wetting fluids such as water which often results in the formation of resistance to the flow in a given conduit. The phenomenon of film or layer has been studied by several researchers from experimental to the analytical standpoint.

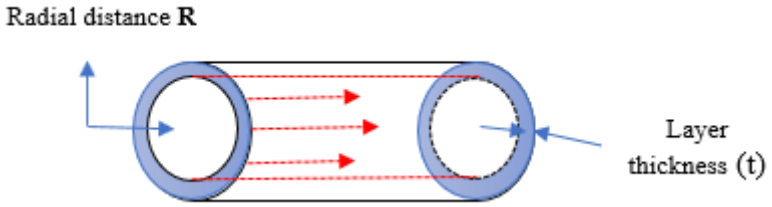

Figure 2: Flow through an idealized capillary tube in porous media

Consider a laminar and immiscible multiphase flow of incompressible fluids in a geometrically idealized capillary tube as in fig.3, the velocity as a function of radial distance with a no-slip boundary condition can mathematically be represented by H-P velocity equation given for flow through pipes as [18]:

$$v(r) = \frac{\Delta P}{4\mu L_T}(R^2 - r^2) \qquad (31)$$

where R is the size (radius) of the capillary, r is the radial position at any given time, v is flow velocity, and other parameters retain their usual meaning as defined previously. By considering the effect of the layer thickness t of a surrounding fluid represented by pale blue color, the flow rate q through the capillary from $(r = 0)\ to\ (r = R - t)$ can be obtained as follows:

$$q = \int_0^{R-t} v(r).2\pi r dr \qquad (32)$$

By substituting (31) into (32) and integrating, the flow rate will be:

$$q = \frac{\pi \Delta P}{8\mu L_T}[R^4 - (2Rt - t^2)^2] \qquad (33)$$

However, by replacing the capillary radius R in terms of diameter λ and substituting (2) for L_T, the flow rate becomes:

$$q = \frac{\pi \Delta P}{128\mu L_s^{D_T} \lambda^{1-D_T}}[\lambda^4 - 16(\lambda t - t^2)^2] \qquad (34)$$

For flow through a given porous media, the total flow rate can be determined from the summation of flow through all capillaries as was previously given by (14). Hence, using the same concept, the total flow is obtained by combining (5) with (34) as follows:

$$Q = \int_{\lambda_{min}}^{\lambda_{max}} \left[\left(\frac{\pi \Delta P}{128\mu L_s^{D_T} \lambda^{1-D_T}}[\lambda^4 - 16(\lambda t - t^2)^2]\lambda_{max}^{D_f} \lambda^{-1-D_f} D_f\right)\right] d\lambda \qquad (35)$$

By integrating and simplifying (35), the total flow Q can be expressed as:

$$\boldsymbol{Q = \frac{\pi \Delta P D_f}{128\mu L_s^{D_T}}\left[\frac{\lambda_{max}^{3+D_T}}{3+D_T-D_f} + \frac{16\lambda_{max}^{1+D_T}((\frac{\lambda_{min}}{\lambda_{max}})^{(1+D_T-D_f)}-1)}{1+D_T-D_f}t^2 + \frac{32\lambda_{max}^{D_T}(1-(\frac{\lambda_{min}}{\lambda_{max}})^{D_T-D_f})}{D_T-D_f}t^3 + \frac{16\lambda_{max}^{D_T-1}((\frac{\lambda_{min}}{\lambda_{max}})^{(D_T-D_f-1)}-1)}{D_T-D_f-1}t^4\right]} \qquad (36)$$

Therefore, combining (36) with Darcy's law and (20), the permeability in the fractal porous media is thus:

$$\boldsymbol{K = \frac{4(2-D_f)\emptyset L_s^{1-D_T}}{128(1-\emptyset)}\left[\frac{\lambda_{max}^{1+D_T}}{3+D_T-D_f} + \frac{16\lambda_{max}^{D_T-1}((\frac{\lambda_{min}}{\lambda_{max}})^{(1+D_T-D_f)}-1)}{1+D_T-D_f}t^2 + \frac{32\lambda_{max}^{D_T-2}(1-(\frac{\lambda_{min}}{\lambda_{max}})^{D_T-D_f})}{D_T-D_f}t^3 + \frac{16\lambda maxDT-3((\lambda min\lambda max)(DT-Df-1)-1)DT-Df-1t4}{}\right]} \qquad (37)$$

(37) is the modified permeability model for flow in fractal porous media in terms of layer/film thickness (t). It can be seen that the permeability K is a function of several parameters such as maximum pore aperture, layer thickness, fractal dimensions and porosity. By utilizing the correlations for D_f, λ_{max}, and $\emptyset$ given by (22a-d) and the relation in (25), the permeability as well as the relative permeability of any flowing phase (wetting or nonwetting) can be computed using the proposed model. However, it is essential to note that the modified model assumes that the fluid at the wall of the capillaries does not move and as such its velocity is zero. Also, the surface diffusion which could become important in the case of gas flow was assumed to be negligible.

5. Results and discussion

In this work, it can be seen that several parameters appear in that appear in the derived models. Therefore, it is crucial to note that the values of the parameters such as porosity, pore sizes, fractal dimension and tortuosity were evaluated using 2D image of Bentheimer sandstone while the remaining variables were obtained from experimental data.

5.1 Fractal analysis of the Bentheimer sandstone image

In this work, two parameters were evaluated in order to describe the fractal characteristics of the studied sandstone. The parameters are pore area and tortuosity fractal dimensions. From the analysis, the pore area fractal dimension D_f was found to be 1.58. The D_f shows the extent to which the sandstone deviates from the standard Euclidian dimension [13] as well as the extent of its heterogeneity [4]. Based on the computed value of D_f, it appears that the analyzed sandstone has a lesser degree of heterogeneity. And this agrees with the reports from several publications that the Bentheimer sandstone is a homogeneous porous material with predominant constituent minerals being feldspar and quartz [20]. Similarly, the tortuosity fractal dimension D_T was calculated as 1.14. The D_T shows how tortuous or convoluted the flow pathways are in the analyzed sandstone image. This portrays the fact that a real porous media does not actually have straight flow paths as is sometimes assumed. Also, the determined tortuosity dimension agrees closely with some reported values for fractal porous media [3]. Moreover, the data truly reflect the behavior of fractal objects whose dimensions are non-integer in nature, and they satisfy the conditions: $1<D_T<2$ and $1<D_f<2$as reported in [3,11]. The significance of D_T in the porous media was examined by incorporating its value in the computation of permeability. And it was found that the permeability decreased by 21.7% when the calculatedD_T was considered.

Additionally, based on the image used in this work, the porosity of the Bentheimer sandstone was found to be 22.3%. This value closely matched the experimental results of 23.2 and 23.5% reported in [20] and [21] respectively. The slight variation observed may be attributed to the fact that the utilized 2D image did not include the contribution of micro-porosity. Another possible reason for the little deviation could be due to low resolution of the segmentation tool which might have made it impossible to capture the tiny pore spaces from the image and as such resulted in the underestimation of the porosity.

5.2 Capillary pressure model analysis

Fig.4 presents the graphical representation of the capillary pressure P_c data as obtained using the formulated model (30a). The model was validated by utilizing published experimental data of the Bentheimer sandstone. Although the core sample used for the laboratory experiment may not be the representative sample of the utilized imaged, the data display a good agreement. This can perhaps be due to the general homogeneous nature of the Bentheimer sandstone. Nonetheless, the values from the analytical solution seem to be a little above those obtained from experiment. The difference can be attributed to the higher porosity (implying larger pores) reported experimentally as compared with the one computed in this work.

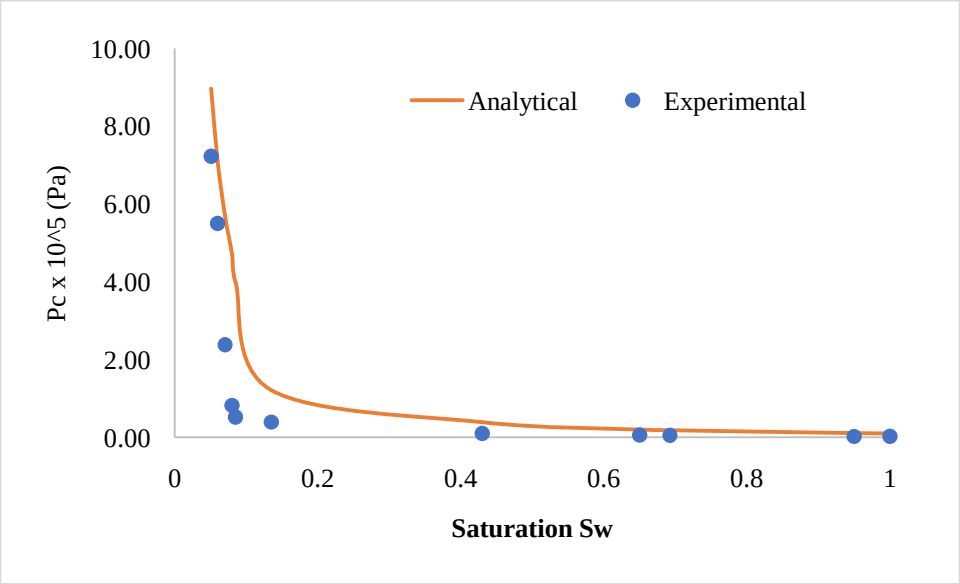

Figure 4: Validation of the capillary pressure model

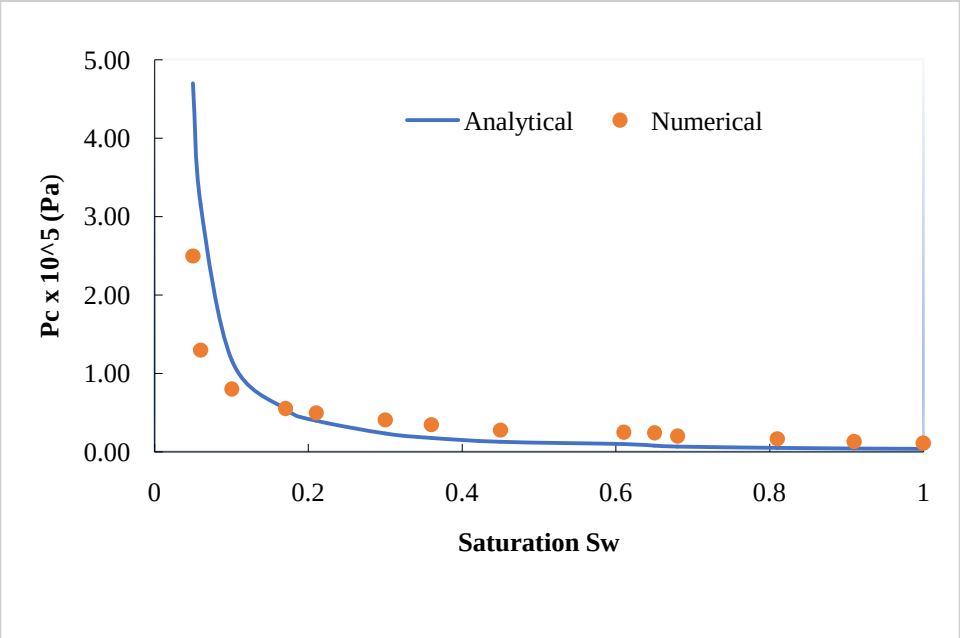

Figure 5: Comparison between analytical and numerical modeling results

Fig.5 shows a comparison between capillary pressure data as determined from the formulated analytical function and numerical data. The calculated curve shows a good agreement with the numerically computed data. The plot was generated for a less water-wet condition with contact angle ($\theta = 40^{o}$). The curve displays an expected trend of capillary pressure being negatively correlated with the saturation of a given phase. It apparently shows that the drainage capillary pressure in Bentheimer sandstone increases with a corresponding decrease in wetting phase saturation S_w. This relation can be ascribed to the fact that as the saturation of nonwetting medium increases, it usually displaces the wetting phase from the larger pores with small capillary pressure into the smaller apertures with a larger capillary pressure. Also, as depicted in (30), capillary pressure has an inverse relationship with pore size, and this implies that when the wetting fluid occupies small pore openings, the capillary pressure becomes increasingly high. Furthermore, as the wetting fluid saturation decrease, its pressure reduces, and this has a resultant effect of increasing the pressure difference (capillary pressure) between the 2-phases.

Moreover, fig.5 exhibits a near flat steep behavior over a wide range of saturation. This observation can be related to the reported homogeneity of the Bentheimer sandstone. Again, it can also be noted that as the wetting phase approaches an irreducible amount, no matter the pressure of the non wetting phase imposed, the capillary curve will only be increasing vertically showing that the wetting fluid has reached an irreducible fraction that cannot be displaced further.

5.3 Relative permeability model analysis

Fig.6 displays the computed relative permeabilities plots as obtained by using the derived models (26) and (27). On a general note, the analytically evaluated curves show a good agreement with the experimentally sourced data. The plots display the variation of the relative conductance of 2-phase (oil and water) in the Bentheimer sandstone as function of saturation. It can be seen that the relative permeability of the wetting medium (water) increases with corresponding increase in saturation of the water, while that of the non wetting component shows a continuous decrease and this is considered to be consistent with known physical situation.

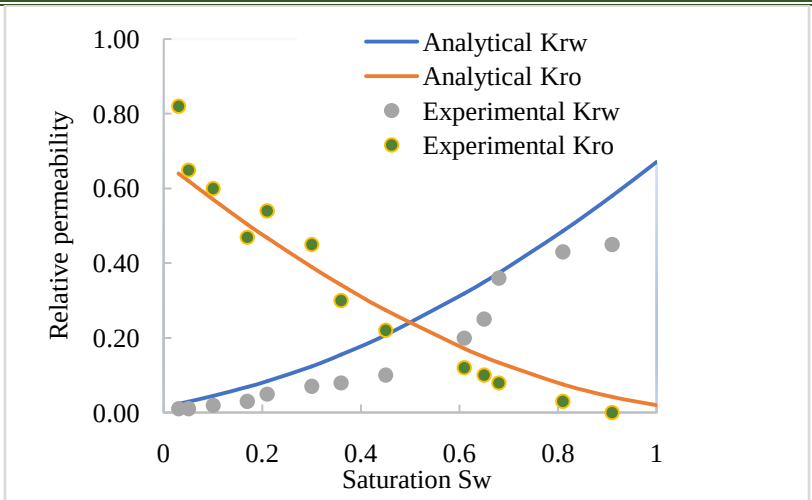

Figure 6: Validation of the relative permeability model

However, while it is evident that the oil phase relative conductance depicts a closer agreement with the experimental result, the wetting phase (water) on the other part shows a wider variation from the reported experimental results. The analytical model seems to have overestimated the relative permeability of the water. One reason that can be ascribed to this contrast is the fact that, unlike in the experimental work where a real core in 3D form was used to simulate the actual flow, the formulated functions utilized values from the 2D SEM image with assumption of perfect circularity of the pores in the sandstone. Also, the Bentheimer sandstone as reported in [20] is water-wet and as such the wetting fluid (water) tends to adhere to the smaller pores with consequent effect of having lower permeability. Furthermore, the capillary openings in the real sandstone that was used could be more tortuous with resultant increase in flow resistance than was assumed in the analytical calculation.

Similarly, the results from the derived models were further compared with simulation results from [22] as shown in fig.7. The compared plots portray similar trend as in the case of the comparison with experimental data. So, it can as well be contended that the apparently large relative permeabilities from the analytical results in comparison with the simulation data are due to the fact that the simulation was also conducted on 3D pore network model which is a similar replication of what happens in the experimental process. However, it is essential to note that the reconstructed 3D pore network model may not necessarily provide complete connectivity and pore sorting (as is the case in real sample). The difference could also be ascribed to the fact that the reconstructed 3D structure may not have used a similar 2D image that was utilized in this work.

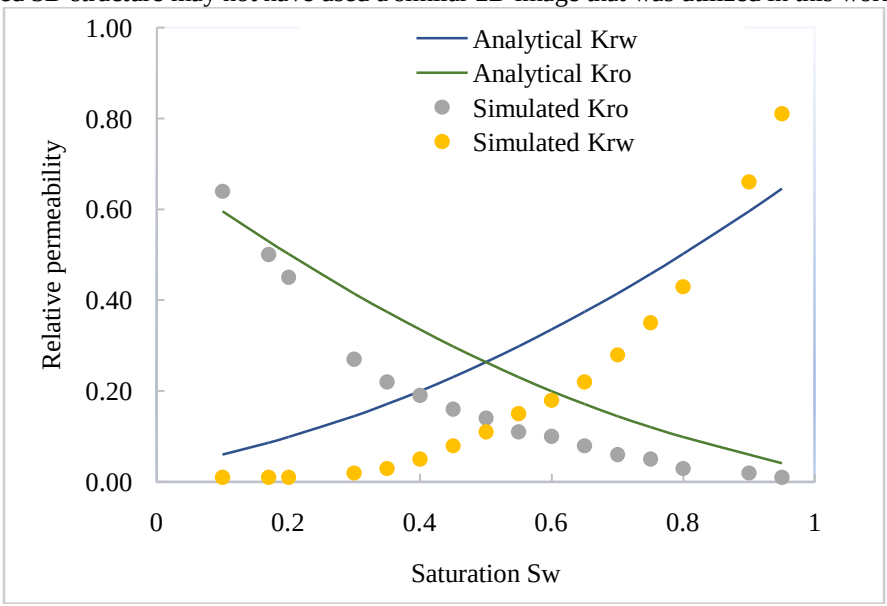

Figure 7: Comparison between analytical and simulation results

5.4 Modified permeability model and the effect of film thickness

Fig.8 depicts a comparison between the 2-phase (oil and water) relative permeability curves as determined using the modified permeability function (37) and experimental values. It can be observed from the figure that the modified model shows a good agreement with existing experimental findings on the relative phase conductance in Bentheimer sandstone. It even appears that there is a stronger agreement between the data calculated using the model (with layer thickness effect) and experimental data as opposed to when the film thickness was not considered (fig.6). This may imply that the model with a layer thickness incorporated gives a better representation of the actual phase relative permeability.

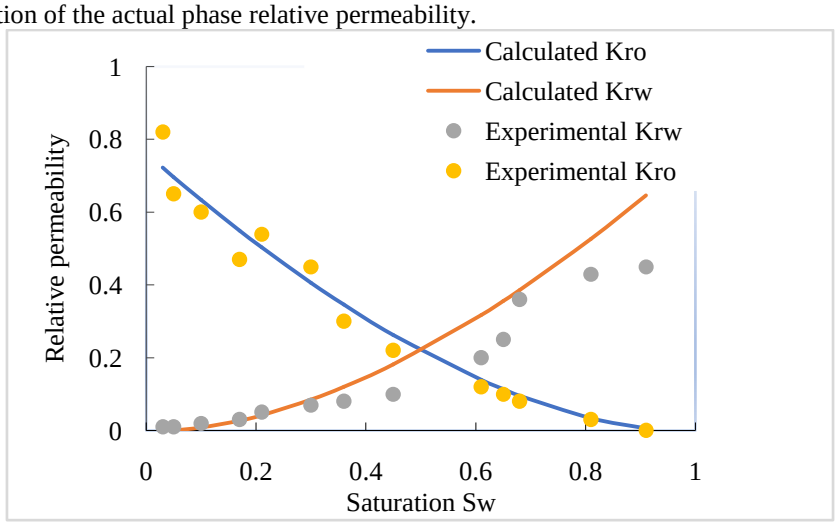

Figure 8: Validation of the modified permeability model

6. Conclusion

In this work, an image-based approach was employed to determine the fractal characteristics of Bentheimer sandstone, and fractal-based relative permeability and capillary pressure expressions were formulated. The functions were tested and validated using the extracted micro structural values and published experimental data. From the analyzed image, the Bentheimer sandstone is relatively homogeneous and exhibits fractal behavior as evidenced by the computed fractal dimensions. The derived capillary pressure and relative permeability functions show good agreement with both experimental and numerical data of the Bentheimer sandstone, and it can logically be concluded that the formulated models can also be applied to other similar sandstones. However, the relative permeability relation was somewhat more consistent with published experimental results for the nonwetting phase (oil), but shows a slight agreement for the wetting medium (water). Hence, the derived function can model nonwetting phase more accurately than the corresponding wetting phase. Also, the modified permeability model that incorporates film/layer thickness shows a more accurate match with experimental data. And based on this, it can be concluded that the model provides a better prediction approach for flow in the analyzed sandstone. Lastly, the developed models showed that both relative permeability and capillary pressure depend not only on saturation but also are functions of microstructural parameters such as (pore size, fractal dimension, porosity, tortuosity), and properties such as (wettability and interfacial tension).

References

[1] Adler, P.M. and Thovert, J.F., (1993). Fractal porous media, *Transport in porous media*, *13*(1), pp.41-78.

[2] Tan, X.H., Liu, J.Y., Li, X.P., Zhang, L.H. and Cai, J., (2015). A simulation method for permeability of porous media based on multiple fractal model, *International Journal of Engineering Science*, *95*, pp.76-84.

[3] Yu, B. and Li, J., (2001). Some fractal characters of porous media, *Fractals*, *9*(03), pp.365-372.

[4] Tan, X.H., Li, X.P., Liu, J.Y., Zhang, G.D. and Zhang, L.H., (2014). Analysis of permeability for transient two-phase flow in fractal porous media, *Journal of Applied Physics*, ***115***(11), p.113502.

[5] Yu, B., Zou, M. and Feng, Y., (2005). Permeability of fractal porous media by Monte Carlo simulations, *International journal of heat and mass transfer*, *48*(13), pp.2787-2794.

[6] Lu, T., Li, Z., Lai, F., Meng, Y., Ma, W., (2018). The effect of flow resistance on water saturation profile for transient two-phase flow in fractal porous media. *Advances in Geo-Energy Research*, 2(1), pp. 63-71.

[7] Xu, P., (2015). A discussion on fractal models for transport physics of porous media. *Fractals*, *23*(03), p.1530001.

[8] Li, K., (2010). More general capillary pressure and relative permeability models from fractal geometry, *Journal of contaminant hydrology*, *111*(1-4), pp.13-24.

[9] Yu, B. and Liu, W., (2004). Fractal analysis of permeabilities for porous media, *AIChE journal*, *50*(1), pp.46-57.

[10] Tan, X.H., Kui, M.Q., Li, X.P., Mao, Z.L. and Xiao, H., (2017). Permeability and porosity models of bi-fractal porous media, *International Journal of Modern Physics B*, *31*(29), p.1750219.

[11] Yu, B. and Cheng, P., (2002). A fractal permeability model for bi-dispersed porous media, *International Journal of Heat and Mass Transfer*, *45*(14), pp.2983-2993.

[12] Chen, X. and Yao, G., (2017). An improved model for permeability estimation in low permeable porous media based on fractal geometry and modified Hagen-Poiseuille flow, *Fuel*, *210*, pp.748-757.

[13] Liu, R., Jiang, Y., Li, B. and Wang, X., (2015). A fractal model for characterizing fluid flow in fractured rock masses based on randomly distributed rock fracture networks, *Computers and Geotechnics*, *65*, pp.45-55.

[14] Othman, M.R. and Helwani, Z., (2010). Simulated fractal permeability for porous membranes, *Applied Mathematical Modelling*, *34*(9), pp.2452-2464.

[15] Cai, J., Perfect, E., Cheng, C.L. and Hu, X., (2014). Generalized modeling of spontaneous imbibition based on Hagen–Poiseuille flow in tortuous capillaries with variably shaped apertures, *Langmuir*, *30*(18), pp.5142-5151.

[16] Y.Zhou,*Pore Scale Modeling of Capillary Pressure Curves in 2D Rock Images*,doctoral diss., University of Stavanger, Norway, 2013.

[17] Xiao, B. and Chen, L., (2013). A Fractal Model for Capillary Pressure of Porous Media, *Research Journal of Applied Sciences, Engineering and Technology*, *6*, pp.593-597.

[18] Wang, J., Song, H., Li, T., Wang, Y. and Gao, X., (2017). Simulating gas-water relative permeabilities for nanoscale porous media with interfacial effects, *Open Physics*, *15*(1), pp.517-524.

[19] Keehm, Y., Mukerji, T. and Nur, A., (2004). Relative Permeability Simulation using the Two-phase Lattice-Boltzmann Method, *5th Conference and Exposition on Petroleum Geophysics 2004,* India, pp. 696-703.

[20] Øren, P.E., Bakke, S. and Arntzen, O.J., (1998). Extending predictive capabilities to network models, *SPE journal*, *3*(04), pp.324-336.

[21] Shikhov, I., d'Eurydice, M.N., Arns, J.Y. and Arns, C.H., (2017). An Experimental and Numerical Study of Relative Permeability Estimates Using Spatially Resolved T1-z NMR, *Transport in Porous Media*, *118*(2), pp.225-250.

[22] Bakke, S. and Øren, P.E., (1997). 3-D pore-scale modelling of sandstones and flow simulations in the pore networks, *SPE Journal*, *2*(02), pp.136-149.

